

Research Article

Investigation of Small-Scaled Soil Structure Model under Earthquake Loads via Small Shaking Table Tests

Mohammed El Hoseny ^{1,2}, Jianxun Ma ¹, Dong Luo ¹ and Yanchao Yue ¹

¹School of Human Settlements and Civil Engineering, Xi'an Jiaotong University, Xi'an 710054, Shaanxi Province, China

²Faculty of Engineering at Shoubra, Benha University, Cairo 11629, Egypt

Correspondence should be addressed to Mohammed El Hoseny; mohammed.elhoseny@stu.xjtu.edu.cn and Jianxun Ma; majx@mail.xjtu.edu.cn

Received 4 July 2022; Revised 16 August 2022; Accepted 29 August 2022; Published 26 September 2022

Academic Editor: Chongqiang Zhu

Copyright © 2022 Mohammed El Hoseny et al. This is an open access article distributed under the Creative Commons Attribution License, which permits unrestricted use, distribution, and reproduction in any medium, provided the original work is properly cited.

This paper aims to determine the appropriate scaling coefficient rigorously in the dynamic analysis of structures via small shaking table tests to represent the full real case while considering the soil-structure interaction problem. In addition, we investigate the seismic effects of the superstructure with flexible and fixed bases. To achieve this purpose, seven stories of concrete moment-resisting frames supported on silty clay soil were scaled. According to the shaking table specifications, a small-scaled soil-structure model was executed with a scaled factor of 1 : 50. Consequently, the scale steel skeleton model was built to represent the real superstructure. In addition, the laminar soil container for the soil block was constructed to reduce undesirable boundary effects. Three earthquakes have been applied at the superstructure base as a fixed base and at the bottom of the soil block in the soil structure system as a flexible base. The numerical simulations are implemented for scaled and real models. According to obtained results from experimental and numerical investigations, the numerical model achieved good results with experimental observation. In addition, the small scaling factor of 1 : 50 can represent the seismic response of full construction conditions with acceptable precision. It is observed that the flexible base has overestimated in lateral displacement of the real superstructure compared with a fixed base, in which the maximum amplification percentage at the roof floor level reaches up to 98% under seismic load. Otherwise, the shear force distribution along the height and base shear of the superstructure with a flexible base decreases compared with a fixed base. The maximum reduction percentage is 38% under seismic load. Consequently, the safety and cost of the superstructure are affected.

1. Introduction

Most civil designer engineers consider the structure's support a fixed base during seismic analysis and design. This assumption is improper because there is an interaction effect between the soil and structure during seismic motions, especially in the presence of weak soil. Therefore, it is imperative to investigate the effects of soil-structure interaction on lateral displacements, shear force distributions of different column locations, and base shear of the superstructure under seismic loads. The significance of the dynamic soil-structure interaction (SSI) is summarized into two components: the inertial component and the kinematic component. Both components are generally affected by the

seismic structural response [1, 2]. Most of the researchers focus on analytical [3–5] and numerical studies [6–9] more than on experimental investigations [10, 11]. Pioneering work was proposed to develop the hybrid numerical method (finite element method, moving particle simulation) to simulate the complex dynamic behavior of structures [12]. The developed numerical method was verified with a series of benchmark problems, whether they were analytical or experimental studies. Other studies [13, 14] performed a full simulation of the centrifuge model using the three-dimensional (3D) discrete-element method (DEM). This model was validated with other physical experimental results to check its effectiveness and accuracy. While in this study [15], they performed large-scale shaking table tests to

investigate the near-fault ground motions effects on the seismic response of slopes. They mainly depended on experimental results. Consequently, numerical and analytical studies without experimental observations may not be convincing in practical engineering. In turn, the validated numerical analyses provide an alternative to experimental observations. Therefore, carrying out a shaking table test considering the SSI effect combined with the corresponding numerical simulation is preferable. Such as in Reference [16], the researchers evaluated the seismic response of reinforced concrete structures by using smart materials along with plastic hinges of the beams to resist the high strain under cyclic and seismic loads. The numerical analyses were performed by the seismo struct model and verified the results with other laboratory reports. The experimental and numerical results were in good agreement. However, this study neglected the effects of SSI under seismic loads. In addition, another study [17] performed a three-dimensional finite element analysis by ANSYS software on a Structure-Soil Structure Interaction (SSSI) test. The numerical model was verified with experimental results to carry out many parametric studies with practical applications in engineering. The large-scale modeling at 1:15 was applied to two buildings with 12-story cast-in-place concrete frames. To reduce the undesirable boundary effects, the soil container was flexible and cylindrical. By comparing the results of numerical simulations with experimental observations, the built modeling is suitable for numerical simulation analyses with other parametric studies. Moreover, in Reference [18], large-scale shaking table tests with a scale factor of 1:4 on a six-story steel frame structure supported on a pile group with SSI effects and on a rigid foundation were performed. The numerical simulation method using ABAQUS software was validated with experimental results. It is concluded that the SSI effects have become more considerable. A series of shaking table tests and theoretical analyses on liquefiable soils in pile group foundations of tall buildings were studied to evaluate the seismic responses of structure, foundation, and soil under major, moderate, and minor earthquakes [19]. They analyzed the results derived from the shaking table tests, including a free-field test, a structure on a rigid foundation test, and a long pile-soil structure. The scaling coefficient applied in this study was 1:10 for a concrete structure cast in place with a 12-story. The seismic responses of a structure with pile SSI are affected and compared with a rigid foundation case. The same researchers [20] performed on 12-story concrete moment resisting frames supported on pile foundations on soft soil and fixed bases to study the dynamic effects of SSI under seismic loads. Large-scale shaking table tests with a scaling coefficient of 1:6 were applied. A shear laminar container was used to minimize the effects of soil boundaries during experiments. The results showed that the effects of SSI have been amplified in lateral displacements and inter-story drifts compared with no SSI effects. In contrast, the inter-story shear force decreases with SSI compared with a fixed base. While reference [21] investigated reinforced concrete buildings with fourteen stories as full-scale in the Republic of Srpska under different

seismic motions. Other researchers [22] applied a full-scale soil-structure simple frame with cross bracings. Most of the mentioned studies with full-scale and large-scale factors are better and more concise. However, such research execution would be difficult due to skilled labor requirements, high-technical instruments, consumption of more time, and high cost.

A few researchers [23, 24] provided other methods to represent the full real soil-structure model via small shaking table capacity with low cost to assess the seismic structure response considering the SSI effects. To achieve this type of research, the derived data from laboratory measurements are compared with numerical simulations to check the accuracy of the results [25]. Consequently, the novelties of this research are to verify adequate accuracy for the appropriate small scaling coefficient of the coupled soil structure system via small shaking table tests under seismic loads. In addition, investigate the seismic response of the superstructure without SSI and with SSI effects. To achieve these issues, a series of experimental studies were performed on a small shaking table at the American University in Cairo (AUC), Egypt. The dimensions of the small shaking table are a width of 1.30 m and a length of 1.70 m. In addition, the maximum carry-over load is five tones.

2. Methodology

2.1. Real Soil-Structure Model System. The real superstructure consists of seven concrete moment-resisting frames with a raft foundation. The total height of the building is 21 m and consists of double bays in both directions. Each direction with a bay span is 4.0 m. The soil layer is silty clay with a unit weight of $\gamma = 17.8 \text{ kN/m}^3$ and a shear wave velocity of 220 m/s. Also, the soil block's length, width, and depth are 70 m, 50 m, and 40 m, respectively. The configuration of the real soil-structure model and sectional plan with concrete dimensions is displayed in Figure 1.

A numerical investigation was carried out by SAP2000 software [26] of a real superstructure with a fixed base, as displayed in Figure 2, to check the safety and adequate section properties. Afterward, conclude the fundamental period of the superstructure and total mass as depicted in Table 1.

2.2. Scaled Soil Structure Model System. To achieve the accuracy measurement from the laboratory tests with the real model, the appropriate geometric scaling coefficient has been determined according to shaking table specifications (dimensions and characteristics). The scaling model is geometric scaling and kinematic or dynamic scaling. Many works of literature verified and checked the geometric and dynamic similitude laws of scaled models with real models [27, 28] and had good agreement results. Therefore, the Cauchy condition presented the similitude laws of the geometric and dynamic scaled models used in shaking table tests [29]. Table 2 shows the similitude laws of geometric and dynamic scaling factors.

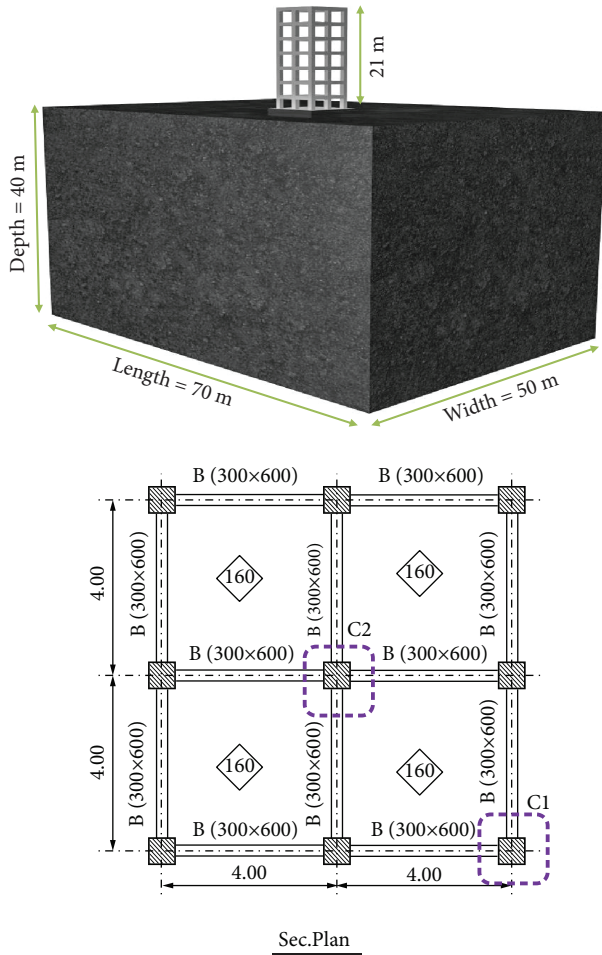


FIGURE 1: Configuration of real soil-structure model.

According to the small shaking table specifications, the appropriate scaling coefficient was chosen to be $\lambda = 1:50$. Therefore, the total height of the scaled superstructure was 0.42 m, and the width in both directions was 0.16 m. The equivalent steel-scaled model was used as an alternate solution to represent the concrete moment resisting frames due to the volume and weight of the concrete. In addition, the length, width, and depth of the soil layer were scaled to be 1.4 m, 1.0 m, and 0.8 m, respectively. For the superstructure, to conclude the time period and total mass of the steel skeleton structure, the real model's time period and total mass in Table 1 should be scaled according to the similitude laws displayed in Table 2. The scaled factor of a time period and mass are $\lambda^{0.5}$ and λ^3 , respectively. Therefore, Table 3 shows the required time period and mass of the scaled superstructure with a fixed base.

A numerical model was built by SAP2000 to conclude the section properties of the steel skeleton to achieve the properties in Table 3. The trial and error method was applied to reach the properties of the steel skeleton structure. Figure 3 presents the final dimensions and section properties of the steel skeleton model with a mild steel grade of 240/350, in which all connections between elements were welded. As a result, the adopted time period and total mass of the superstructure are shown in Table 4. It is noted that the

maximum difference between the adopted and required properties of the superstructure does not exceed 1.9% in the mass item. Consequently, the scaled model was manufactured in the workshop.

2.2.1. Scaled Soil Properties. The soil layer cannot be placed directly on the shaking table. Therefore, many researchers [30, 31] described a laminar soil container to represent the soil boundary and maintain the soil layer as a real condition. According to similarity rules, the scaled geotechnical model's length, width, and depth were 1.40 m, 1.00 m, and 0.80 m, respectively. The material components of the laminar shear box consisted of aluminum and rubber layers that were joined by a high-strength resin material. The use of aluminum material is due to possessing ductile properties and low weight [32, 33]. In addition, the wood plate was fixed at the level of the shaking table.

To conclude the dimensions of the aluminum and rubber sections, the natural frequency of the laminar shear box is matched with the natural frequency of the soil block to prevent any waves from an interface between container and soil during seismic excitations, which was determined as 9.43 Hz. Therefore, the laminar shear box was manufactured in the workshop, as shown in Figure 4. The soil properties used in this research are shown in Table 5 [28].

2.3. Earthquake Records. Three seismic displacement time histories with different frequency contents, such as Kobe (1995), Northridge (1994), and Chi-Chi (1999) earthquakes, are applied at the bottom of the soil in the soil structure model system and the base of the superstructure in the fixed base case. Scaled displacement time histories were concluded according to similitude laws in Table 2. Therefore, real and scaled displacement time histories are displayed in Figures 5–7, in addition to the characteristics of the real earthquakes [34].

3. Experimental Investigations

3.1. Seismic Response of Scaled Structure Model without and with SSI Effects. Firstly, it is essential to check the time period of the scaled superstructure without SSI effects (fixed base) that matched with numerical analyses before being exposed to seismic motions. Therefore, the scaled structure was put on the shaking table and fixed with four bolts with a diameter of 16 mm (4M16). The LVDT (Linear Variable Differential Transformer) was set up at the roof floor level to measure the response of the superstructure (as shown in Figure 8). A sine sweep test was implemented to check the scaled model's time period. The first resonance between the shaking table and the scaled model indicated the scale model's time period.

Consequently, the time period of the scaled superstructure with a fixed base was 0.0869 seconds, which matched with the numerical analysis in Table 4. Afterward, three different scaled earthquakes were applied at the base of the structure. The lateral displacement obtained from the experimental investigation at the roof floor level was an absolute lateral displacement that represented the displacement of the shaking table (earthquake motion) plus the

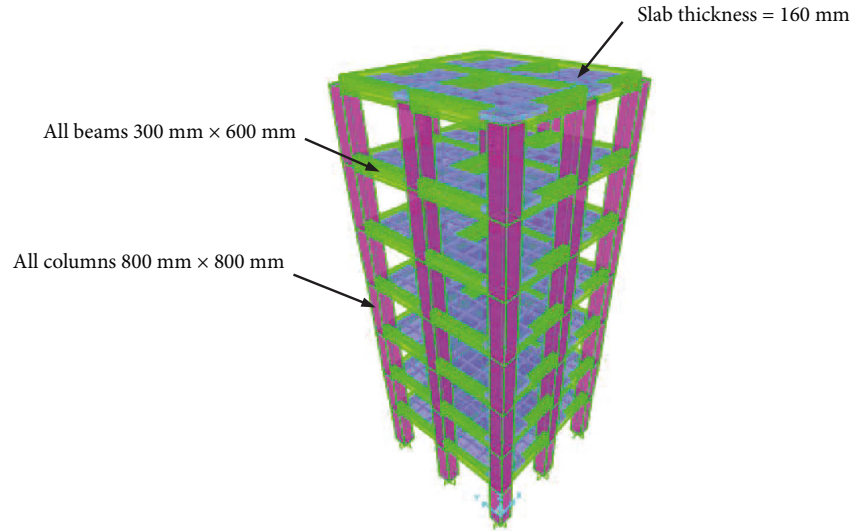


FIGURE 2: Real superstructure with fixed base by SAP2000 software.

TABLE 1: Time period and total mass of the superstructure with a fixed base.

| | |
|----------------------|-------|
| Time period (second) | 0.617 |
| Total masses (tones) | 645 |

TABLE 2: Similitude laws of the geometric and dynamic scaling factor.

| | |
|---------------------|------------------|
| Mass density | 1 |
| Stiffness | λ^2 |
| Force | λ^3 |
| Modulus | λ |
| Strain | 1 |
| Time | $\lambda^{0.5}$ |
| Shear wave velocity | $\lambda^{0.5}$ |
| Frequency | $\lambda^{-0.5}$ |
| Acceleration | 1 |
| Stress | λ |
| Length | λ |
| Mass | λ^3 |

TABLE 3: Required time period and total mass of the scaled superstructure with a fixed base.

| | |
|----------------------|-------|
| Time period (second) | 0.087 |
| Total masses (Kg) | 5.16 |

relative displacement of the superstructure (distortion displacement).

For the SSI case, the laminar soil container was placed on the shaking table and fixed by 14M16 after placing the soil layer. Afterward, the scaled structure was placed in the determined place in the middle of the soil. Finally, LVDT was placed at the roof floor level as in the fixed base case. Figure 9 depicts the scaled soil-structure system in the laboratory. Before applying the three scaled earthquakes, a sine sweep test was performed at the resonance frequency at the shaking table to obtain the scaled model's time period. Therefore, the time period of the superstructure with a flexible base was approximately 0.095 seconds.

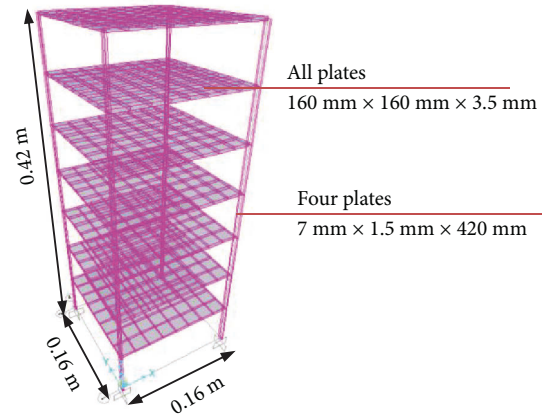


FIGURE 3: Dimension and section properties of steel skeleton.

TABLE 4: Adopted time period and total mass of the scaled superstructure with a fixed base.

| | |
|----------------------|-------|
| Time period (second) | 0.086 |
| Total masses (Kg) | 5.06 |

It is observed that the flexible base has been amplified in the time period by 9.3% in comparison with the fixed base case.

Three scaled seismic waves were applied at the base of the soil block level. The absolute lateral displacements were produced at roof floor level, including the movement of the input motion, a rocking component due to foundation rotation, and a relative lateral displacement of the superstructure (distortion component).

4. Numerical Approaches

4.1. *Seismic Response of Real and Scaled Structure Models without and with SSI Effects.* Numerical analyses were carried out to verify the experimental investigation. In addition, simulate other parametric studies to evaluate the SSI effects compared with a fixed base. By referring to the real and

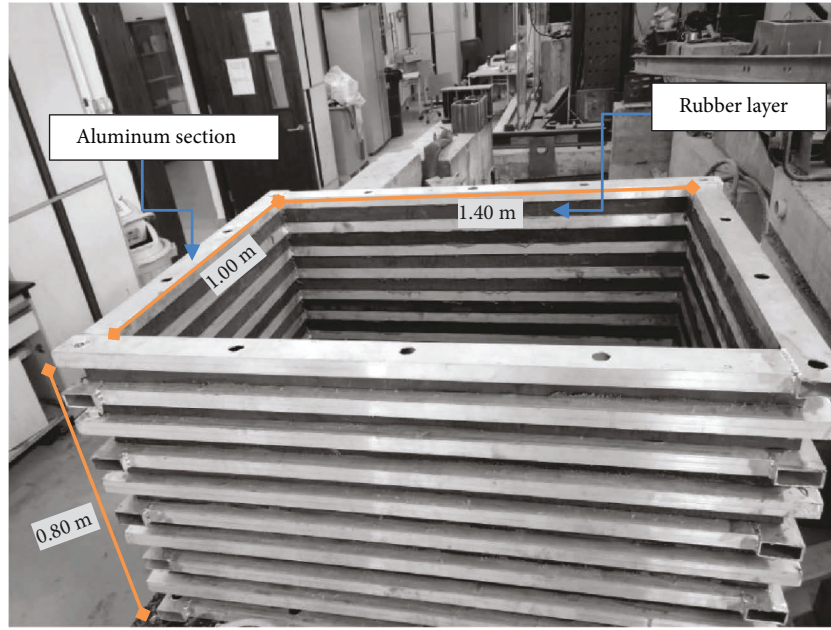


FIGURE 4: Laminar shear box.

TABLE 5: Soil properties for scaled SSI system.

| Parameter | Symbol | Magnitude | Unit |
|---------------------------|----------|-----------|-------------------|
| Average unit weight | γ | 17.8 | kN/m ³ |
| Young modulus | E | 4571 | kN/m ² |
| Shear modulus | G | 1758 | kN/m ² |
| Compression wave velocity | V_p | 58.23 | m/s |
| Shear wave velocity | V_s | 31.13 | m/s |
| Poisson's ratio | ν | 0.3 | — |
| Cohesion | c | 60 | kN/m ² |
| Dilatancy angle | ψ | 1.8 | (degree) |
| Friction angle | ϕ | 31.8 | (degree) |

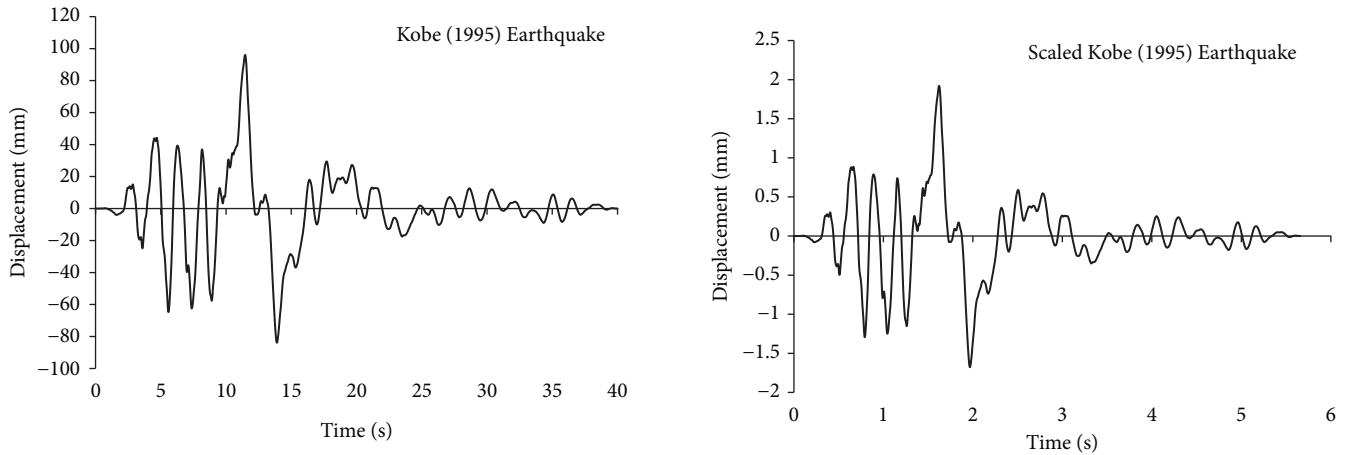
scaled numerical models with fixed bases in Sections 2.1 and 2.2, three seismic motions were applied at the fixed bases of the superstructure. Therefore, the absolute lateral displacements at each floor level for real and scaled models were obtained.

For the SSI case, 3D numerical models with a flexible base were built by PLAXIS 3D software [35] for real and scaled models. The direct method was applied, considering the soil and structure during seismic motions in one step. This model consisted of structural elements, soil blocks, the interface between soil and structure elements, boundary conditions, and input motion. The structure elements consist of slab elements as plate elements and beams and columns as beam elements with the mentioned properties in Sections 2.1 and 2.2. In addition, the soil modeling in this study was the Mohr–Coulomb (MC) criteria (linear-elastic perfectly plastic), for which many researchers [10, 28] had good results for this model. The soil layer properties of the scaled model system are given in Table 5. By applying the similitude laws in Table 2, the properties of the real soil layer are concluded. The

interface model properties between soil and structure elements are the same as soil blocks with a reduction factor of 0.67, as mentioned in the PLAXIS manual [35]. The appropriate boundaries were set up in the soil block, in which the soil in the natural case is infinity in all lateral directions. Therefore, free field boundaries with damping dashpots were applied to the lateral boundaries of the soil block to absorb any reflecting seismic waves. The base of the soil block was assumed to be the bedrock base where earthquake loads were employed, as in Figure 10. Therefore, after applying three seismic motions at the bottom of the soil block, the absolute lateral displacements at each floor level under three seismic scenarios for real and scaled models were investigated.

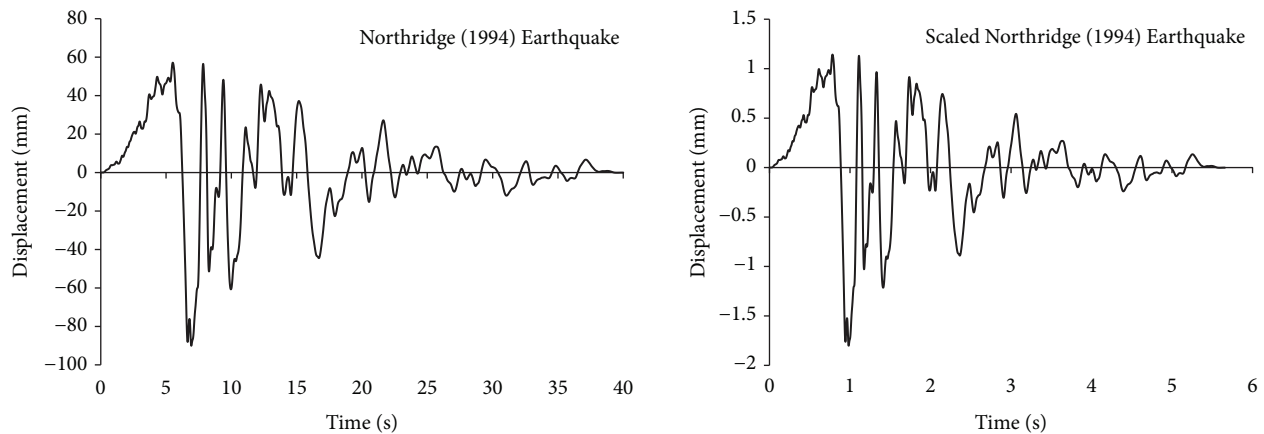
5. Results and Discussion

5.1. Verification of Experimental and Numerical Simulation. Firstly, in this section, the scaled model's numerical analyses and experimental investigations are verified in terms of maximum absolute lateral displacement under different frequency contents



| Earthquake | Country | Date | PGA (g) | Mw (R) | Duration (s) | Station |
|------------|---------|----------|---------|--------|--------------|----------|
| Kobe | Japan | Jan.1995 | 0.34 | 6.9 | 40 | KAKOGAWA |

FIGURE 5: Original and scaled Kobe (1995) earthquake.



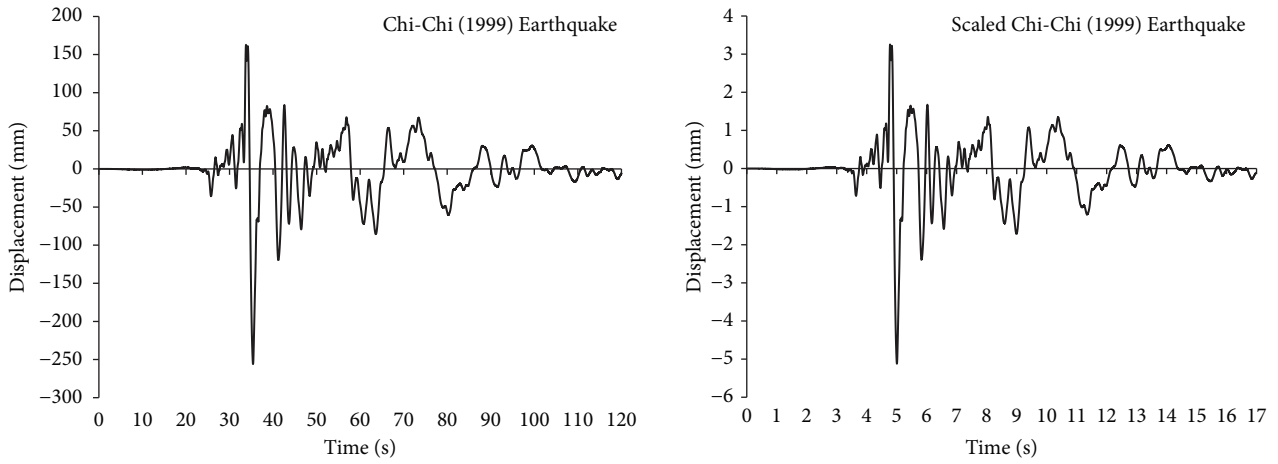
| Earthquake | Country | Date | PGA (g) | Mw (R) | Duration (s) | Station |
|------------|---------|----------|---------|--------|--------------|-----------------------|
| Northridge | USA | Jan.1994 | 0.57 | 6.7 | 40 | CDMG STATION 24278 |

FIGURE 6: Original and scaled Northridge (1994) earthquake.

of earthquakes. Therefore, Figures 11 and 12 display the maximum absolute lateral displacements along the height derived from numerical analyses with experimental results at the roof floor level under scaled earthquakes for fixed and flexible bases, respectively. It is noted that the experimental and numerical results at roof level are adequate and achieve high accuracy. The maximum deviation between experimental and numerical results at the roof level is 4% in both conditions: fixed and flexible bases.

After ensuring that the experimental and numerical results of the scaled model were in very good agreement with high accuracy, the second phase in the verification is to check the

appropriate scaling coefficient, achieving good results in the dynamic analyses. To perform this process, the maximum absolute lateral displacement of the real model is divided by the maximum absolute lateral displacement of the scaled model at each floor level of the superstructure under three seismic motions for each case: fixed and flexible bases. Figure 13 displays the maximum absolute lateral displacements of the real model derived from numerical analyses at each floor level with fixed and flexible bases that showed the effects of SSI compared with the fixed base case. By performing the division process, Figures 14(a) and 14(b) exhibit the resulting inverse scaling coefficients ($1/\lambda$) along the height of the superstructure under



| Earthquake | Country | Date | PGA (g) | Mw (R) | Duration (s) | Station |
|------------|---------|----------|---------|--------|--------------|---------|
| Chi-Chi | Taiwan | Sep.1999 | 0.36 | 7.6 | 120 | CHY006 |

FIGURE 7: Original and scaled Chi-Chi (1999) earthquake.

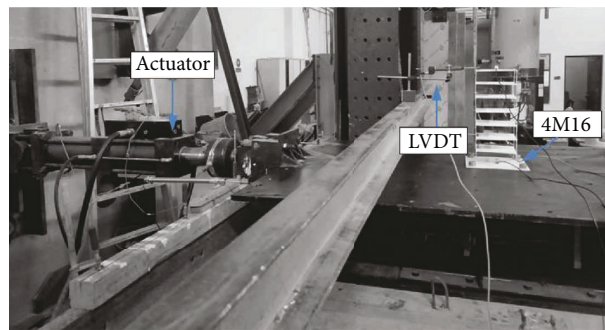


FIGURE 8: Scaled structure fixation on shaking table and LVDT installation.

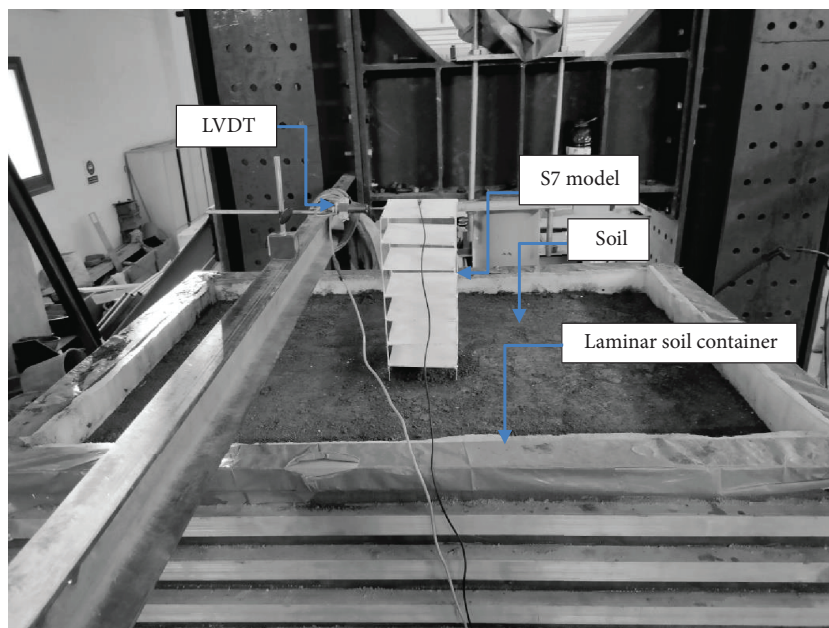


FIGURE 9: Scaled soil-structure interaction system.

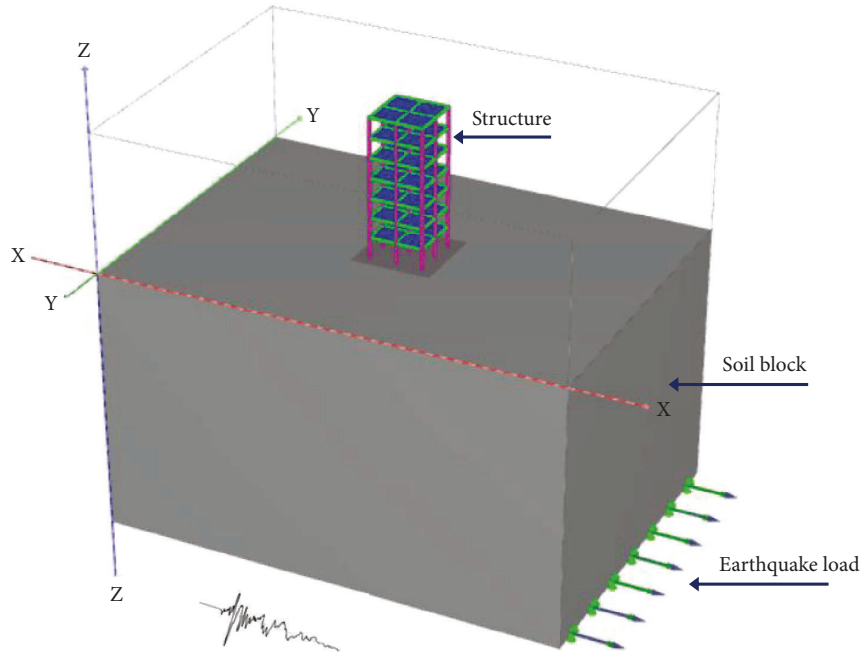


FIGURE 10: Soil structure interaction model by PLAXIS.

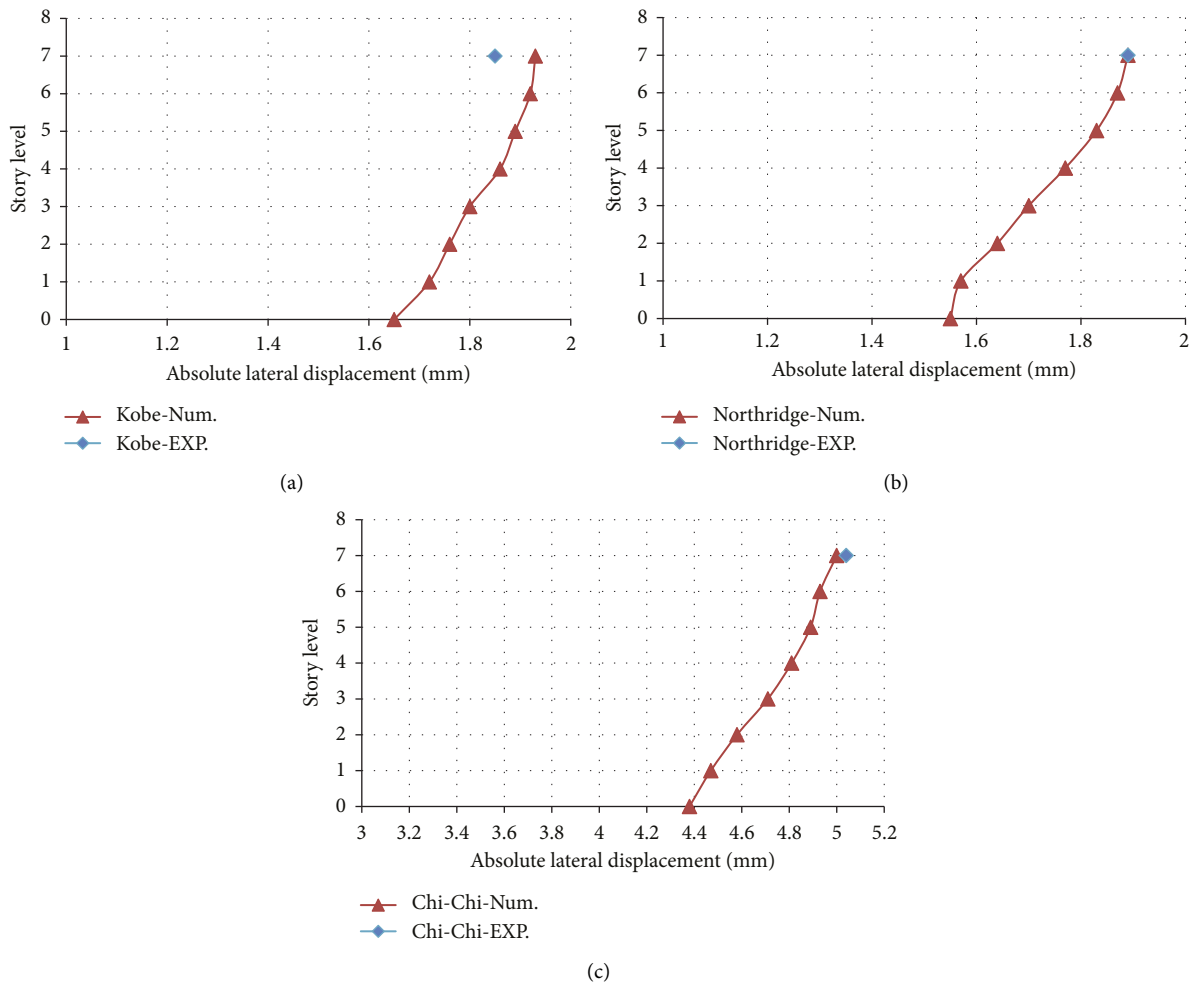


FIGURE 11: Maximum absolute lateral displacements derived numerically and experimentally in a fixed base case under three scaled earthquakes: (a) Kobe. (b) Northridge. (c) Chi-Chi.

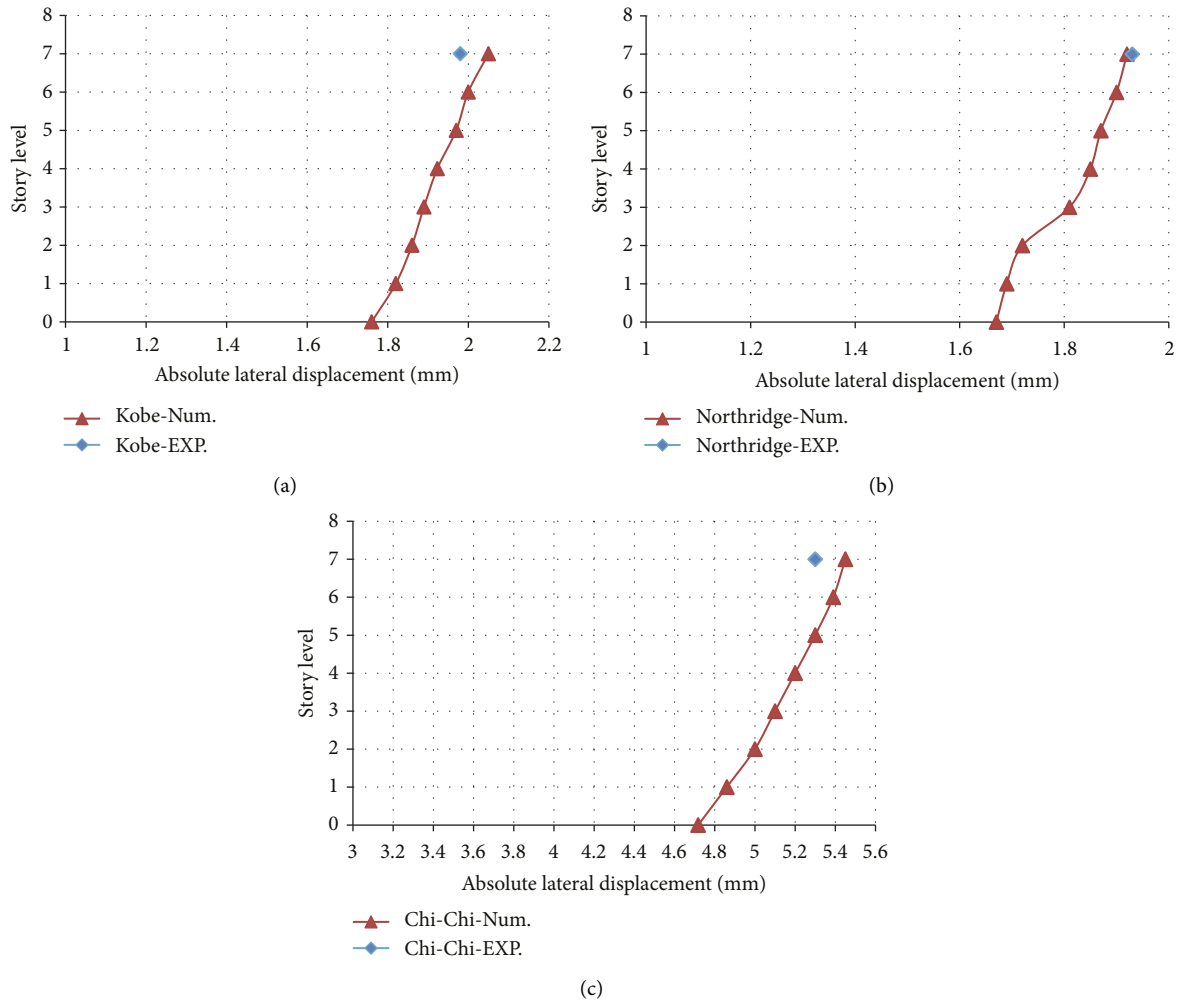


FIGURE 12: Maximum absolute lateral displacements derived numerically and experimentally in a flexible base case under three scaled earthquakes: (a) Kobe. (b) Northridge. (c) Chi-Chi.

three earthquakes for fixed and flexible bases cases, respectively. The target scaling coefficient used in this study was 1:50. Therefore, it is observed that the maximum scaling coefficient is 1:58 in a fixed base case under the Chi-Chi and Kobe earthquakes that occurred at the foundation level. While under the Northridge earthquake, the maximum scaling coefficient is 1:61 at the roof floor level. Consequently, the selected scaling factor of 1:50 achieves adequate accuracy under three seismic motions along the height of the superstructure with a fixed base. In the flexible base case, the maximum scaling coefficient along the height of the superstructure is 1:59 under Chi-Chi and Kobe earthquakes that occurred at the foundation level. While under the Northridge earthquake, the values of the scaling coefficient are considered good results from the foundation level to the fourth level (less than 1:60). However, the maximum scaling coefficient under the Northridge earthquake is 1:67 at the roof floor level.

Generally, the selected scaling coefficient of 1:50 is regarded as a suitable scaling factor in the seismic analysis to represent the full-scale real construction model under different seismic scenarios.

5.2. Relative Lateral Displacements of the Superstructure. After ensuring the adequacy of the numerical model, it is suitable to study other parametric to investigate the seismic response of a real superstructure with flexible and fixed bases under different seismic scenarios. The previous results derived from experimental and numerical investigations were absolute lateral displacement that included the movement of the earthquake, relative lateral displacement of the structure (distortion component) that was different in flexible about fixed bases, and a rocking component due to foundation rotation in the flexible base case only. Because the movement of the earthquake is the conjoint movement in both fixed and flexible bases, the displacement time histories at each floor level will be subtracted from the displacement time histories of earthquakes. For example, Figures 15 and 16 show the absolute displacement time histories at the roof floor level with different seismic motions and the resulted relative displacement after subtraction at each time step for fixed and flexible bases, respectively. The resulting relative displacement time histories may be in phase, out-

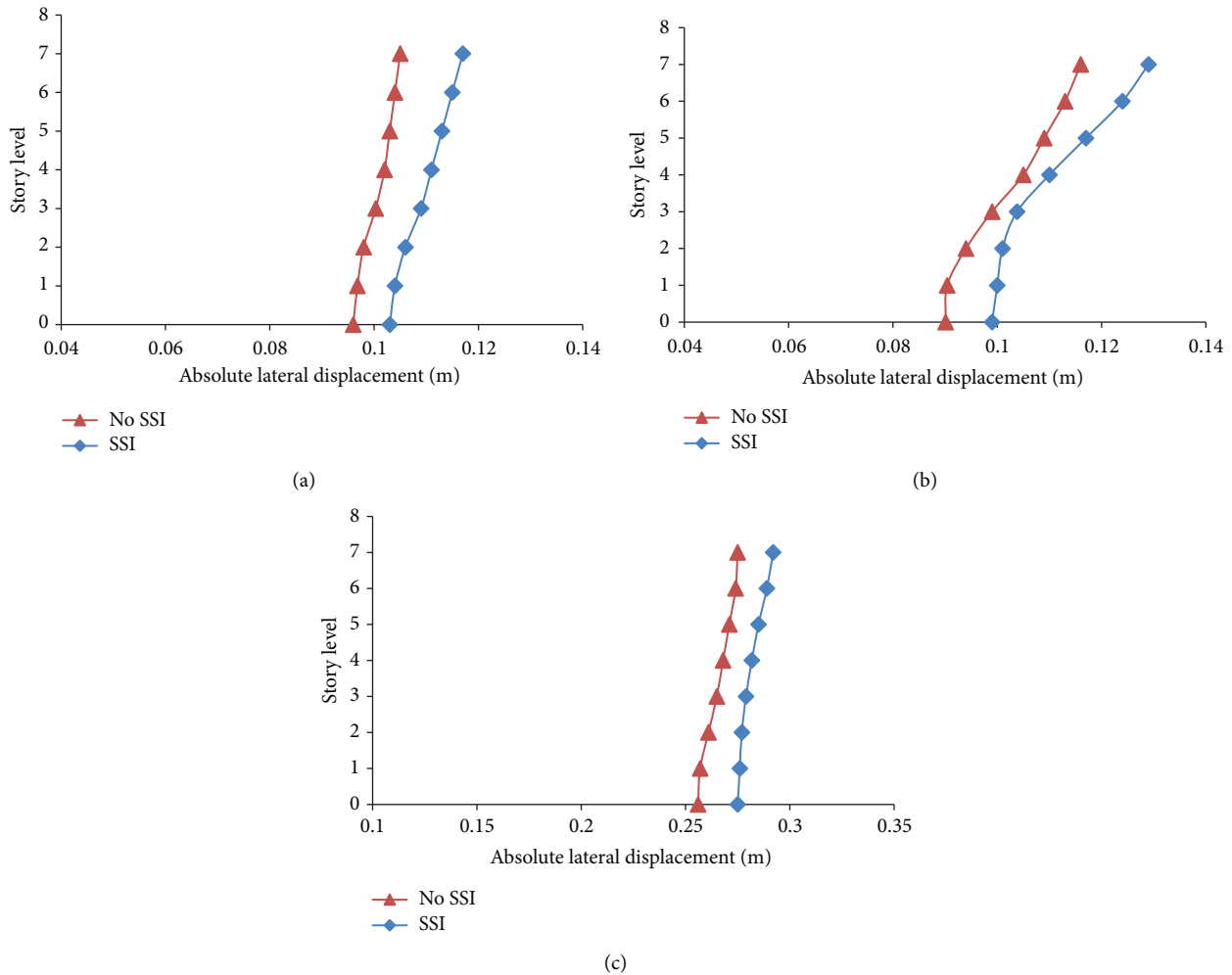


FIGURE 13: Maximum absolute lateral displacement at each floor level with flexible and fixed bases under three real earthquakes: (a) Kobe. (b) Northridge. (c) Chi-Chi.

of-phase, the same sign, or different from absolute and seismic motion time histories.

Consequently, the relative lateral displacement is considered to study the effects of SSI and is compared with a fixed base. Figures 17 displays the maximum relative lateral displacement at each floor level of the real superstructure with fixed and flexible cases under different earthquakes. It is observed that the flexible base has amplified lateral displacement at the roof floor level by 98% under Kobe, 74% under Northridge, and 58% under the Chi-Chi earthquakes. Therefore, the fixed base is unsuitable to represent the structures support under seismic loads, and the fixed base assumption is underestimated in lateral displacement. Consequently, the safety of the superstructure is affected.

5.3. Shear Force Distribution and Base Shear of the Superstructure. The shear force distribution and base shear are important to analyze and design the structural elements of the superstructure due to earthquake loads. Therefore, Figures 18 and 19 display the maximum

envelope shear force distribution along the height of external and internal columns of the superstructure with different support conditions under three seismic loads, respectively. For the external column (C1), it is noted that the flexible base has reduced shear force distribution along the height of the superstructure compared with a fixed base case. The reduction percentages at the base level are 19%, 9%, and 38% under the Kobe, Northridge, and Chi-Chi earthquakes, respectively. While for the internal column (C2), the shear force distribution for the fixed base at the first-floor level to the foundation level is different compared with the flexible base. It may be referred to as its support condition and position. Generally, it is also noted that the flexible base has a reduced shear force distribution along the height compared with the fixed base case. The reduction percentages at the foundation level are 1%, 5%, and 26% under the Kobe, Northridge, and Chi-Chi earthquakes, respectively.

Finally, Figure 20 presents the maximum envelope base shear force for the superstructure under three seismic loads with flexible and fixed bases. It is noted that the flexible base has reduced base shear compared with a

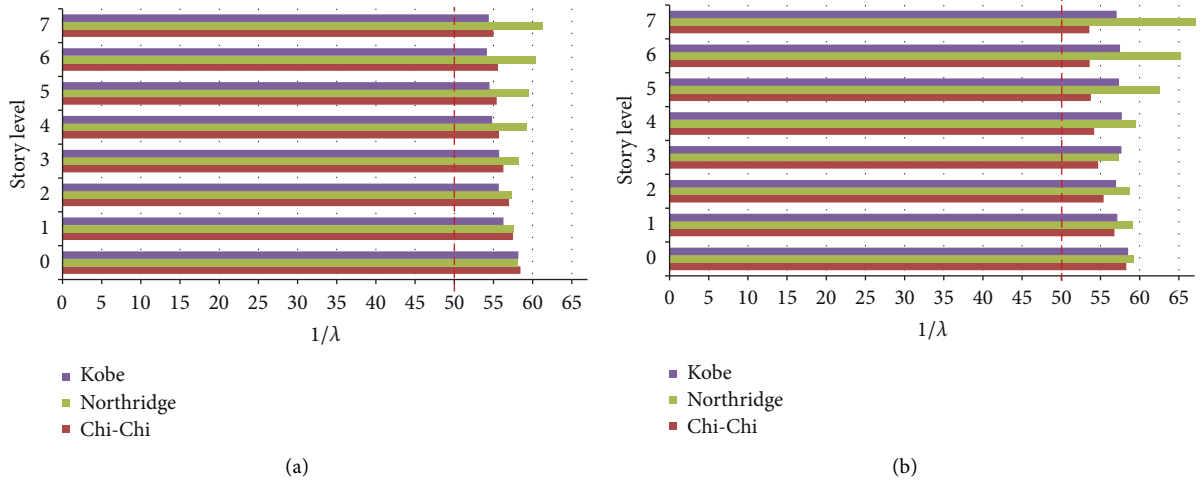


FIGURE 14: Resulting the inverse scaling coefficients ($1/\lambda$) at each floor level of the superstructure under three earthquakes in the cases: (a) fixed base, (b) flexible base.

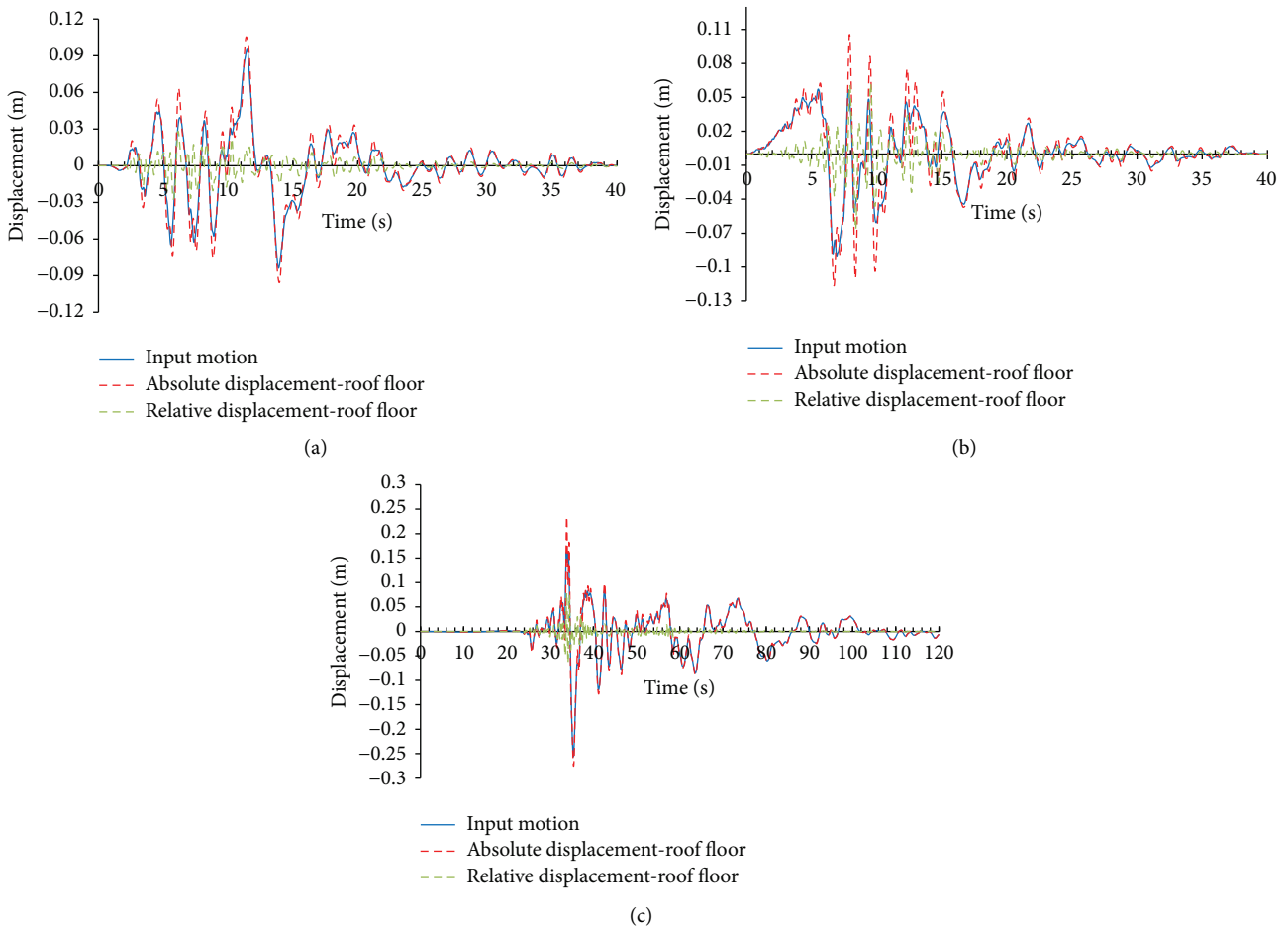


FIGURE 15: Lateral displacement time histories at the roof floor and the superstructure base (input motion) with a fixed base under three real earthquakes: (a) Kobe. (b) Northridge. (c) Chi-Chi.

fixed base under different seismic loads. The reduction percentages are 2%, 12.5%, and 37.5% under the Kobe, Northridge, and Chi-Chi earthquakes, respectively. Consequently, the fixed base is considered improper to

represent the structure’s support under seismic scenarios, and the fixed base assumption is overestimated in shear force distribution and base shear force. Therefore, the cost of the superstructure is affected.

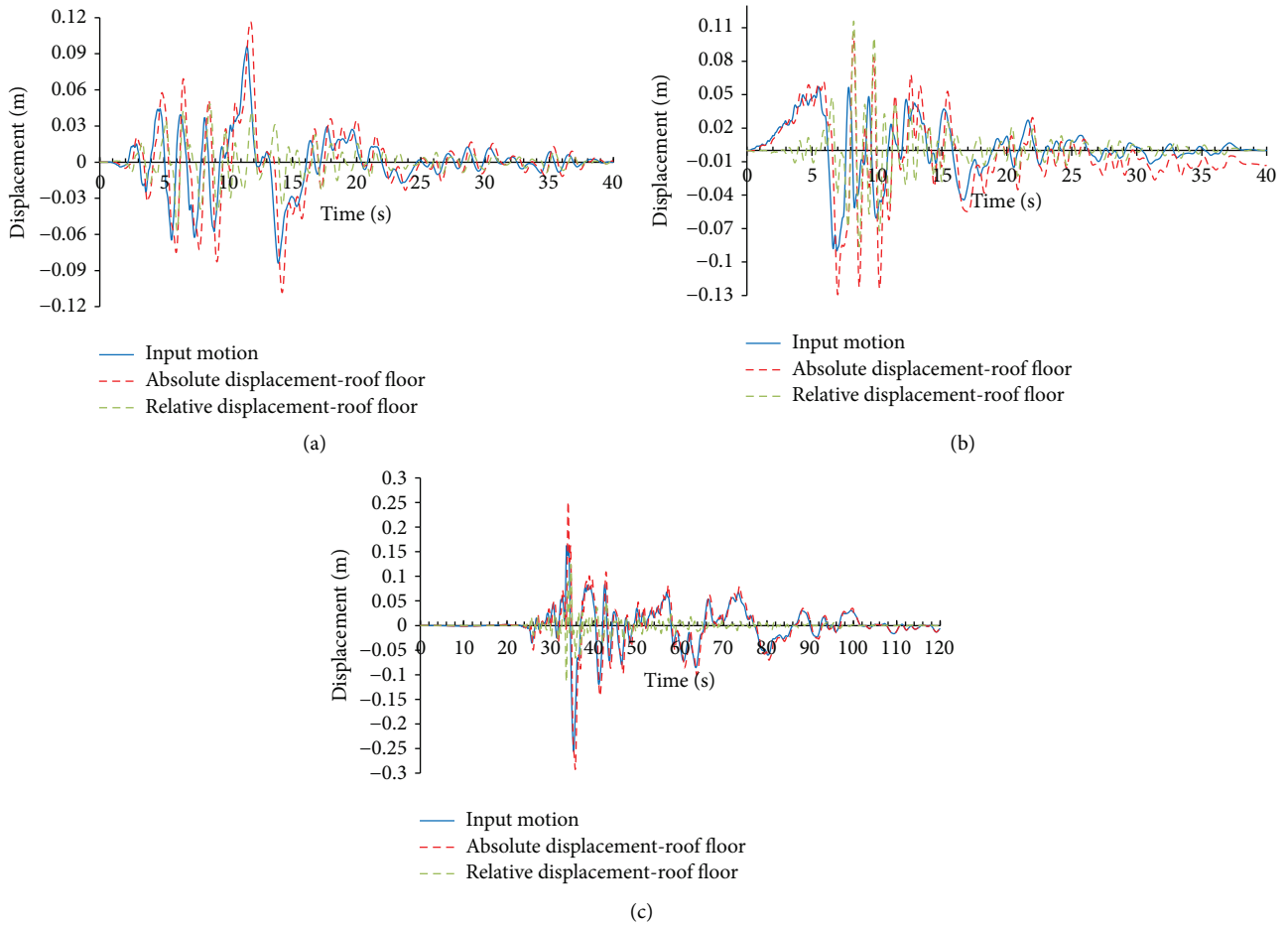


FIGURE 16: Lateral displacement time histories at the roof floor level and the soil block base (input motion) with flexible base under three real earthquakes: (a) Kobe. (b) Northridge. (c) Chi-Chi.

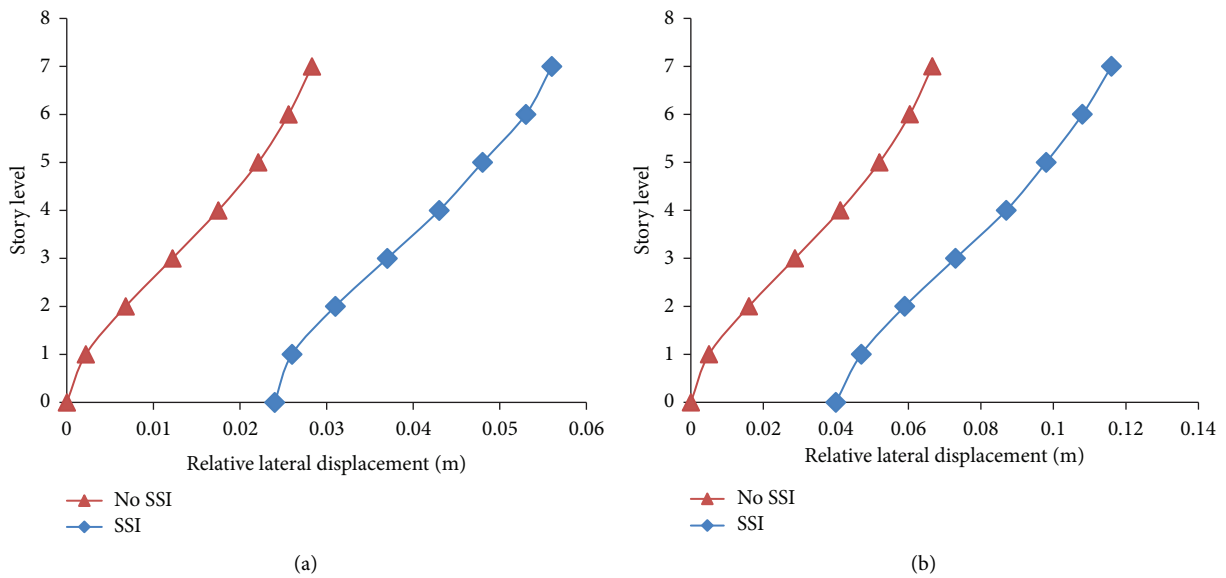


FIGURE 17: Continued.

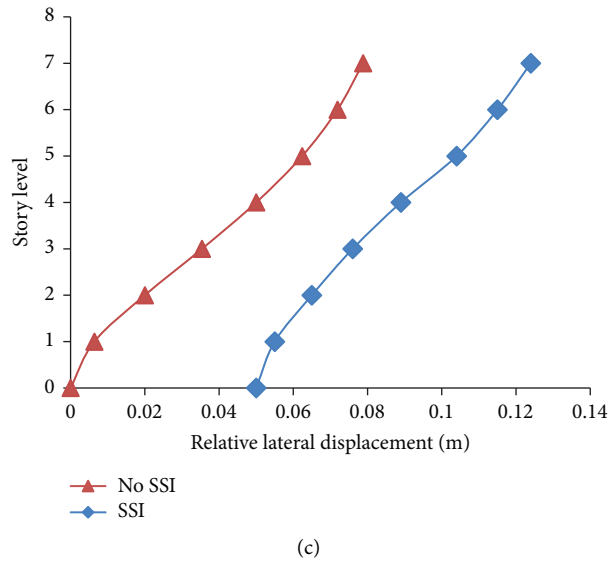


FIGURE 17: Maximum relative lateral displacements at each floor level of the real superstructure without and with SSI effects under three earthquakes (a) Kobe. (b) Northridge. (c) Chi-Chi.

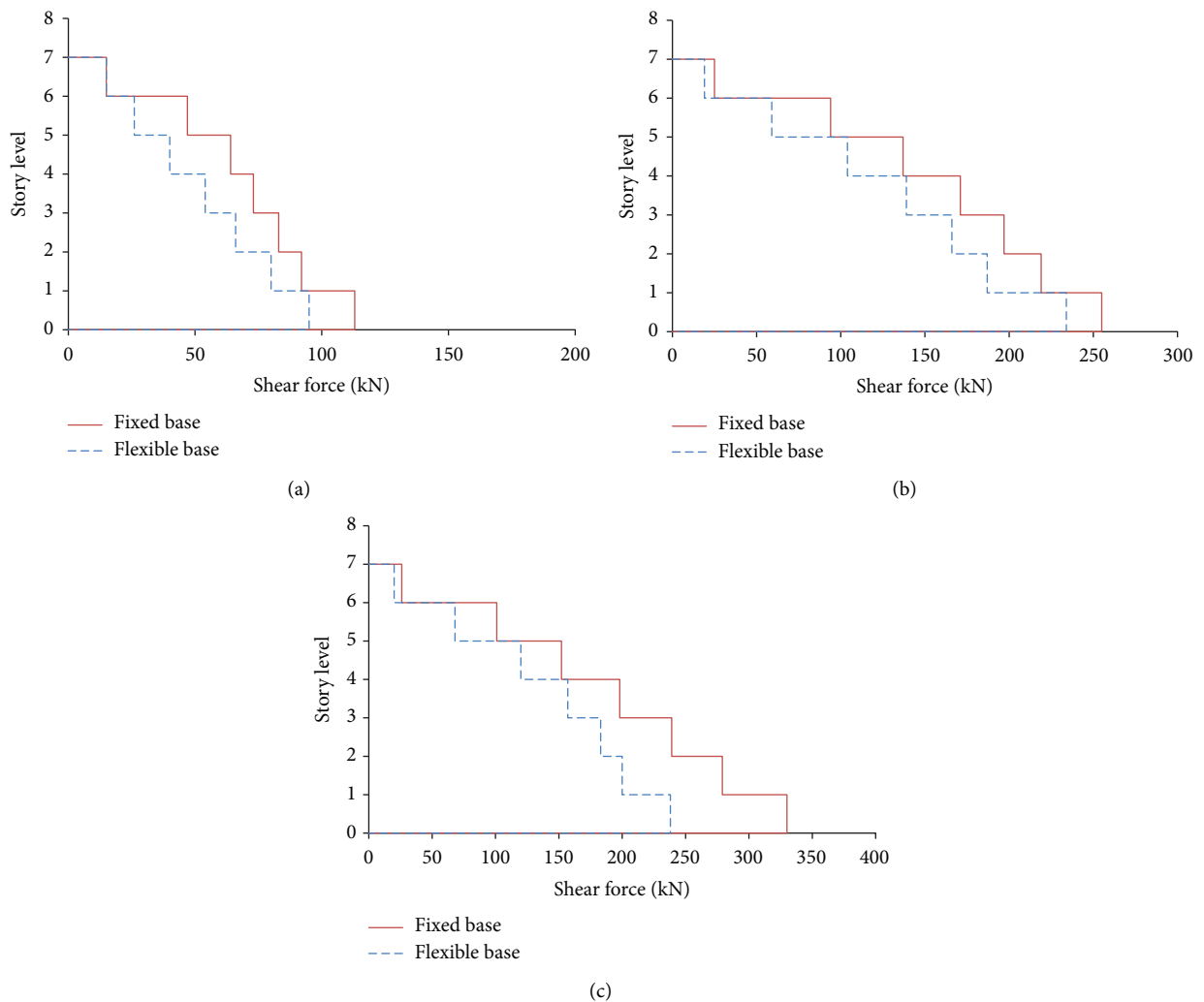


FIGURE 18: Maximum envelope shear force distribution of external column (C1) at the corner along the height for superstructure with flexible and fixed bases under three earthquakes: (a) Kobe. (b) Northridge. (c) Chi-Chi.

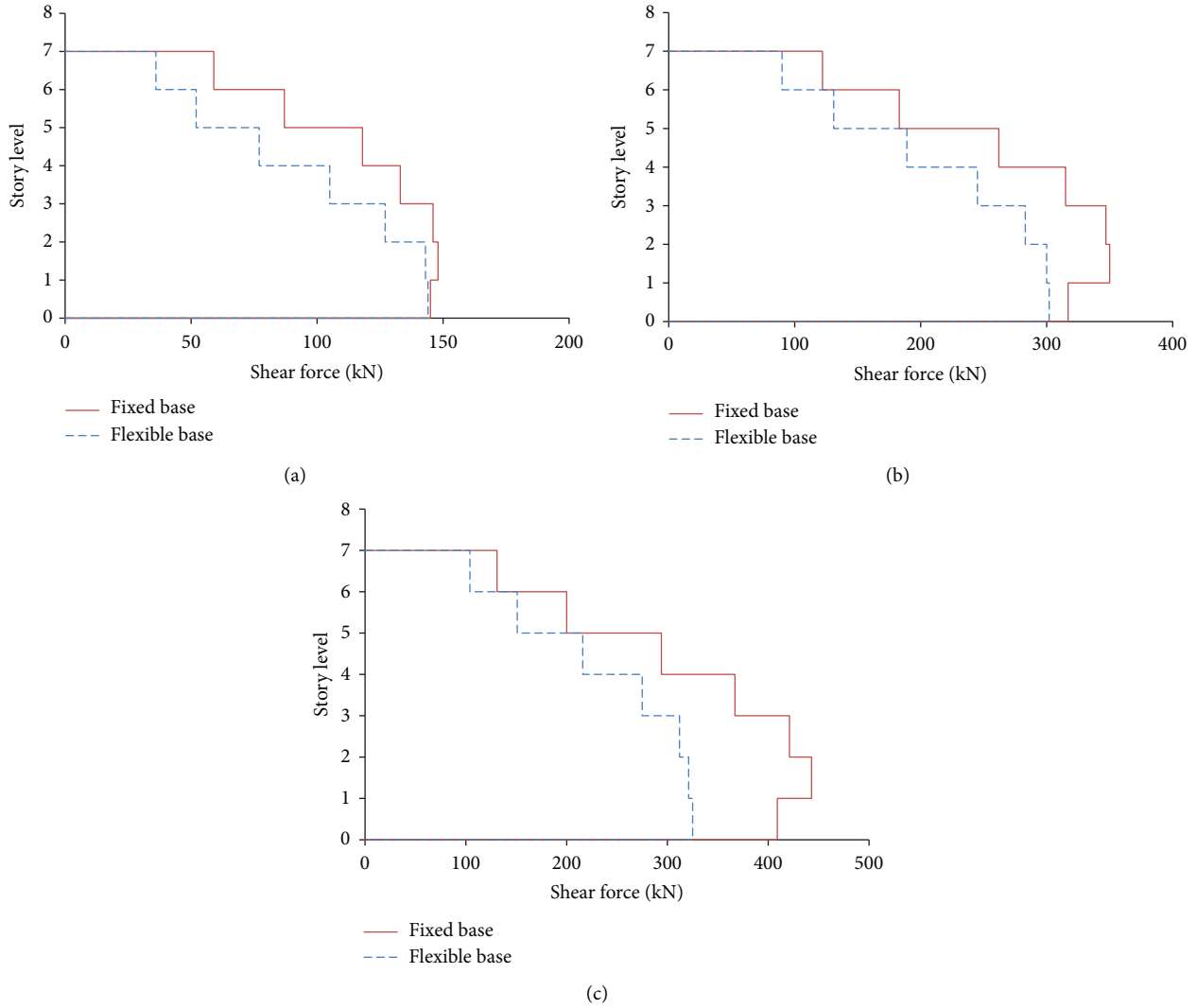


FIGURE 19: Maximum envelope shear force distribution of internal column (C2) at the internal along the height for superstructure with flexible and fixed bases under three earthquakes: (a) Kobe. (b) Northridge. (c) Chi-Chi.

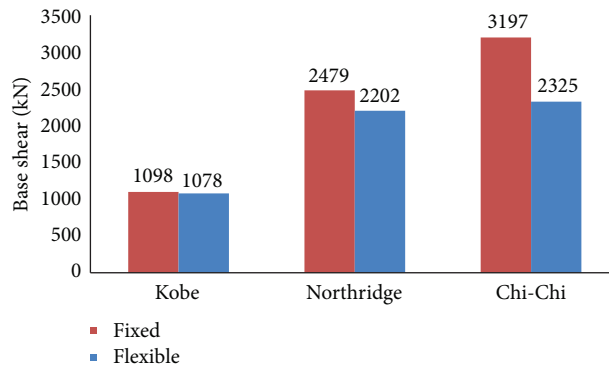


FIGURE 20: Maximum envelope base shear force at the base of the superstructure with flexible and fixed bases under three earthquakes.

6. Conclusions

This paper uses experimental observations and numerical simulations to study the soil structure model on a small

shaking table under seismic loads. In addition, investigate the seismic response of the superstructure with flexible and fixed bases. Seven stories of concrete moment-resisting frames rested on silty clay soil with a shear wave

velocity of 220 m/s were scaled. The scale coefficient applied in this study was 1 : 50, according to the specifications of the shaking table. Consequently, a steel-scaled structure model was manufactured. In addition, a laminar soil container was implemented to decrease undesirable boundary effects. The seismic loads were applied at the base of the superstructure with a fixed base and at the bottom of the soil block in the flexible base case. The numerical simulations were verified with experimental investigations to ensure the adequacy of the numerical model. Afterward, verified the adequacy of the appropriate scaling coefficient in the seismic analyses. Finally, the seismic behavior of the real model with fixed and flexible bases was discussed in terms of relative lateral displacement, shear force distributions for external and internal columns, and base shear of the superstructure under different seismic loads.

The results derived from the numerical analysis of the scaled model were very accurate with experimental measurements under three scaled seismic motions. In addition, the selected scaling coefficient of 1 : 50 achieved accepted accuracy in the dynamic analysis under different frequency contents. It is observed that the flexible base had amplified lateral displacement compared with the fixed base. Subsequently, the fixed base assumption was underestimated in lateral displacement compared with soil deposits. Consequently, the safety of the superstructure is affected. Otherwise, the flexible base reduced the shear force distribution of external and internal columns and the base shear of the superstructure compared with the fixed base. Therefore, the fixed base assumption was overestimated in the shear force distribution and base shear of the superstructure. Consequently, the cost is affected.

Data Availability

The data used to support the findings of this study are available from the corresponding author upon request.

Conflicts of Interest

The authors declare that they have no conflicts of interest regarding the publication of this paper.

Acknowledgments

This work was supported by the construction laboratory at the American University in Cairo (AUC), Egypt, and Omar El Kadi, the authors thank them for supporting them in this laboratory. This research was funded by the National Natural Science Foundation of China (NSFC), grant no. 51178390.

References

- [1] J. Lysmer, T. Udaka, C. Tsai, and H. B. Seed, *FLUSH-A Computer Program for Approximate 3-D Analysis of Soil-Structure Interaction Problems*, California Univ, California, CA, U.S.A, 1975.
- [2] J. P. Stewart, R. B. Seed, and G. L. Fenves, *Empirical Evaluation of Inertial Soil-Structure Interaction Effects*, Pacific Earthquake Engineering Research Center Univ. of California, Berkeley, CA, U.S.A, 1998.
- [3] M. Novak and Y. O. Beredugo, "Vertical Vibration of Embedded Footings," *Journal Of the Soil Mechanics And Foundations Division*, vol. 98, pp. 1291–1310, 1972.
- [4] R. J. Apsel and J. E. Luco, "Torsional response of rigid embedded foundation," *Journal of the Engineering Mechanics Division*, vol. 102, no. 6, pp. 957–970, 1976.
- [5] H. U. Kim, J. G. Ha, K. W. Ko, and D. S. Kim, "Optimization of Two Soil-Structure Interaction Parameters Using Dynamic Centrifuge Tests and an Analytical Approach," *Sustainability*, vol. 12, 2020.
- [6] R. Scarfone, M. Morigi, and R. Conti, "Assessment of Dynamic Soil-Structure Interaction Effects for Tall Buildings: A 3D Numerical Approach," *Soil Dynamics And Earthquake Engineering*, vol. 128, Article ID 105864, 2020.
- [7] D. Forcellini, "A Novel Framework to Assess Soil Structure Interaction (SSI) Effects with Equivalent Fixed-Based Models," *Applied Sciences*, vol. 11, Article ID 10472, 2021.
- [8] F. Castelli, S. Grasso, V. Lentini, and M. S. V. Sammito, "Effects of Soil-Foundation-Interaction on the Seismic Response of a Cooling tower by 3D-FEM Analysis," *Geosciences*, vol. 11, p. 200, 2021.
- [9] D. Forcellini, "Soil-structure Interaction Analyses of Shallow-Founded Structures on a Potential-Liquefiable Soil deposit," *Soil Dynamics And Earthquake Engineering*, vol. 133, Article ID 106108, 2020.
- [10] F. Goktepe, M. Sahin, and E. Celebi, "Small shaking table testing and numerical analysis of free-field site response and soil-structure oscillation under seismic loading," *Bulletin of Engineering Geology and the Environment*, vol. 79, no. 6, pp. 2949–2969, 2020.
- [11] S. H. R. Tabatabaiefar, B. Fatahi, and B. Samali, "Numerical and experimental investigations on seismic response of building frames under influence of soil-structure interaction," *Advances in Structural Engineering*, vol. 17, no. 1, pp. 109–130, 2014.
- [12] C. Zhu, Z. Chen, and Y. Huang, "Coupled moving particle simulation–finite-element method analysis of fluid–structure interaction in geodisasters," *International Journal of Geomechanics*, vol. 21, no. 6, 2021.
- [13] B. Zhang, Y. Huang, and C. Zhu, "Flow–structure interaction mechanism under coriolis conditions," *Journal of Engineering Mechanics*, vol. 147, no. 4, 2021.
- [14] Y. Huang, B. Zhang, and C. Zhu, "Computational assessment of baffle performance against rapid granular flows," *Landslides*, vol. 18, pp. 485–501, 2021.
- [15] C. Zhu, H. Cheng, Y. Bao, Z. Chen, and Y. Huang, "Shaking table tests on the seismic response of slopes to near-fault ground motion," *Geomechanics and Engineering*, vol. 29, pp. 133–143, 2022.
- [16] H. Jahangir and M. Bagheri, "Evaluation of seismic response of concrete structures reinforced by shape memory alloys," *International Journal of Engineering*, vol. 33, pp. 410–418, 2020.
- [17] P. Li, S. Liu, Z. Lu, and J. Yang, "Numerical Analysis of a Shaking Table Test on Dynamic Structure-Soil-Structure Interaction under Earthquake Excitations," *Structural Design Of Tall And Special Buildings*, vol. 26, pp. 1–13, 2017.
- [18] S. Liu, P. Li, W. Zhang, and Z. Lu, "Experimental Study and Numerical Simulation on Dynamic Soil-Structure Interaction under Earthquake Excitations," *Soil Dynamics And Earthquake Engineering*, vol. 138, Article ID 106333, 2020.

- [19] P. Li, J. Yang, and Z. Lu, "Shaking table test and theoretical analysis of the pile–soil–structure interaction at a liquefiable site," *The Structural Design of Tall and Special Buildings*, vol. 27, no. 15, 2018.
- [20] J. Yang, P. Li, and Z. Lu, "Large-scale shaking table test on pile-soil-structure interaction on soft soils," *The Structural Design of Tall and Special Buildings*, vol. 28, no. 18, pp. 1–19, 2019.
- [21] M. D. Trifunac, M. I. Todorovska, M. I. Manić, and B. D. Bulajic, "Variability of the fixed-base and soil--structure system frequencies of a building—the case of Borik-2 building," *Structural Control and Health Monitoring*, vol. 17, no. 2, pp. 120–151, 2010.
- [22] C. Amendola, F. de Silva, A. Vratisikidis, D. Ptilakis, A. Anastasiadis, and F. Silvestri, "Foundation Impedance Functions from Full-Scale Soil-Structure Interaction Tests," *Soil Dynamics And Earthquake Engineering*, vol. 141, Article ID 106523, 2021.
- [23] D. Ptilakis, M. Dietz, D. M. Wood, D. Clouteau, and A. Modaressi, "Numerical simulation of dynamic soil-structure interaction in shaking table testing," *Soil Dynamics and Earthquake Engineering*, vol. 28, pp. 453–467, 2008.
- [24] K. T. Chau, C. Y. Shen, and X. Guo, "Nonlinear Seismic Soil-Pile-Structure Interactions: Shaking Table Tests and FEM Analyses," *Soil Dynamics And Earthquake Engineering*, vol. 29, pp. 300–310, 2009.
- [25] X. Lu, X. Yin, and H. Jiang, "Shaking table scaled model test on a high-rise building with CFT frame and composite core wall," *European Journal of Environmental and Civil Engineering*, vol. 17, no. 8, pp. 616–634, 2013.
- [26] SAP, *Integrated Finite Element Analysis and Design of Structures Graphic User Interface Manual*, Computers and Structures, Inc, Berkley, CA, U.S.A, 2000.
- [27] F. Goktepe, E. Celebi, A. Jawad, and A. J. Omid, "Numerical and Experimental Study on Scaled Soil-Structure Model for Small Shaking Table Tests," *Soil Dynamics And Earthquake Engineering*, vol. 119, pp. 308–319, 2019.
- [28] M. El. Hoseny, J. Ma, and M. Josephine, "Effect of Embedded Basement Stories on Seismic Response of Low-Rise Building Frames Considering SSI via Small Shaking Table Tests," *Sustainability*, vol. 14, p. 1275, 2022.
- [29] P. D. Moncarz, *Theory and Application of Experimental Model Analysis in Earthquake Engineering*, stanford university, Stanford, CA, U.S.A, 1981.
- [30] W. M. Cheung, X. Qin, N. Chouw, T. Larkin, and R. Orense, "Experimental and Numerical Study of Soil Response in a Laminar Box," in *Proceedings of the 2013 NZSEE Conference*, New Zealand, April 2013.
- [31] S. H. R. Tabatabaiefar, *Determining seismic response of mid-rise building frames considering dynamic soil-structure interaction*, PhD Thesis, OPUS, England, U.K, 2012.
- [32] Y. Wang, M. Tayyebi, and A. Assari, "Fracture toughness, wear, and microstructure properties of aluminum/titanium/steel multi-laminated composites produced by cross-accumulative roll-bonding process," *Archives of Civil and Mechanical Engineering*, vol. 22, pp. 49–14, 2022.
- [33] R. Srinivasan, M. Kamaraj, D. Rajeev, S. Ravi, and N. Senthilkumar, "Plasma Spray Coating of Aluminum–Silicon–MWCNT Blends on Titanium Grade 5 Alloy Substrate for Enhanced Wear and Corrosion Resistance," *Silicon*, vol. 14, 2022.
- [34] PEER, *PEER 2010 PEER Strong Motion Database*, University of California, Berkeley, CA, U.S.A, 2010.
- [35] R. B. Brinkgreve, *Plaxis 3D*, plaxis bv, Netherland, 2012.